Modeling of thermal expansion and metallurgical phases of a material during its cooling

A. CLARISSOU[1], V. BRUYERE[2], P. NAMY[2], I. CRASSOUS[1]

1. FRAMATOME, 60 Avenue Paul Girod, UGINE, France
2. SIMTEC, 5 rue Felix Poulat, GRENOBLE, France

Abstract

In metallurgy, the use of numerical models is popular because of the many coupled physical phenomena that occur during the various processes. For instance, the resulting shape and metallurgical state of a material are very sensitive to changes in temperature. The ingot cooling leads to thermal contraction: the thermal exchanges are drastically affected by the quality of contact between the metallic ingot and the crucible. To better understand these phenomena, a 2D axisymmetric model is developed using COMSOL Multiphysics® to simulate the casting and cooling of an ingot in a crucible. The casting process is carried out until the ingot has reached its final height, and then the ingot is cooled for several hours by water flowing over the crucible walls. By using a moving mesh method to describe the growth of the ingot, a thermo-mechanical model is built which includes the metallurgic phases evolution. After numerical validation, this model can be used to predict the influence of thermal contact resistances at the external walls of the ingot on the temperature and shape evolution of a material during casting. The metallurgical phase composition of the metal ingot is directly influenced by its thermal history over time and the properties of each potential phase change : this model can be used to describe the evolution of the different metallurgical phases during the cooling.

Keywords: Heat Transfer, Metallurgy, Contact Resistances, Solid Mechanics, Thermal Dilatation

Introduction

Numerical modelling is a very useful tool to increase the control of foundry processes and to predict the metallurgical and mechanical properties of molten metal ingots. In FRAMATOME, various melting processes are used. For example, the Creusot plant produce large forging and castings products in carbon steel or stainless steel which are required to manufacture the primary components of a nuclear power plant. At Ugine plant, the vacuum arc remelting process is used to produce Zirconium alloys ingots with a high level of quality in terms of chemical composition and solidification structures. Finally, the vacuum induction melting is used in several laboratories to produce and study alloys and melting processes.

The objective of this work is to develop a model able to describe crucible filling through a simplified approach and to study in details ingot-crucible interactions to predict their influence on the resulting metallurgy. Different physical phenomena are of primary importance, such as the cooling mode and the contact conditions between the ingot and the crucible.

Modeling and Governing Equations

Each "physics" used in COMSOL Multiphysics® is detailed with the different assumptions used in this work. For confidentiality reasons, the geometry is simplified in this paper and arbitrary dimensions have been chosen. A 2D axisymmetric geometry is built, consisting of a mold or crucible (in grey in Figure 1) and an ingot (in red in Figure 1). Material properties are obtained from the literature for steel for the ingot [1], and copper for the crucible. The radius of the ingot, initially liquid and thus filling the volume, is considered equal to the radius of the crucible. The filling phase is simplified here, and the volume of the ingot will grow as a function of time, with a moving mesh method and a free surface, during the simulation. Depending on the type of casting process and the mass of the ingot, the filling can be slow (several hours) or fast (less than 1 minute). The cooling mode can also vary greatly depending on the application. As a study case, different configurations will be simulated in this work. Fluid flow will not be taken into consideration here (for the filling and in the molten metal) but could be easily added in a future work thanks to COMSOL Multiphysics® flexibility.
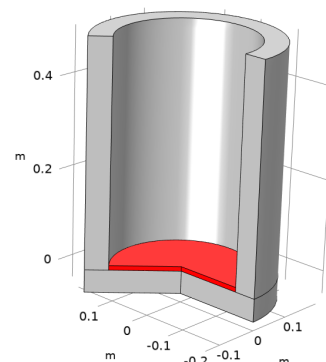

Figure 1. 2D axisymmetric geometry

Thermal Exchanges

The transient heat equation is solved in the ingot and in the mold to obtain the temperature field at each point as a function of time:

$$\rho C_p \frac{\partial T}{\partial t} + \nabla \cdot (-k\nabla T) = 0 \qquad \text{Eq. 1}$$

where T is the temperature, ρ the density, k the thermal conductivity and C_p the heat capacity of the material.

At the upper boundary of the ingot, the heat flux is prescribed to maintain the temperature close to the melting point. It represents the input energy from the casting. Concerning the ingot/crucible interfaces, "thermal contact" boundary conditions are used, resulting in a temperature discontinuity. They play a major role in the evolution of the temperature in the ingot and its resulting metallurgy. The boundary heat fluxes q_i from the ingot (1) and from the crucible (2) are related to the temperatures of each boundary T_i through the following relations:

$$-\boldsymbol{n}_1 \cdot \boldsymbol{q}_1 = -h_{ingot}(T_2 - T_1) \qquad \text{Eq. 2}$$
$$-\boldsymbol{n}_2 \cdot \boldsymbol{q}_2 = -h_{ingot}(T_1 - T_2) \qquad \text{Eq. 3}$$

with a heat transfer coefficient h_{ingot} to calibrate.

This coefficient is of prior importance because it directly governs the ingot cooling. Depending on the type of casting, it can be divided in different zones [2]:

- The first zone is the direct contact between the liquid ingot and the crucible. This zone is very limited in size and very high value of conductance can be considered here:
  $h_{ingot} = 10^4 \ \frac{W}{m^2 \cdot K} \ if \ T_1 > T_{liquidus}.$
- The second zone is a transitional zone, where the metal temperature is lower than the liquidus temperature, called the "mixed zone". The contact is not perfect but is made through a succession of asperities and gas pockets. The value of the conductance in this zone is very difficult to estimate but still very important for the process modeling. A constant value of $h = 800 \ \frac{W}{m^2 \cdot K}$ is used and this value will be studied in this work.
- The third zone is defined by a total loss of contact due to heat shrinkage of the ingot. Heat transfer occurs exclusively by radiation, described with the following conductance, with ε_1 the ingot emissivity and σ the Stefan-Boltzmann constant:
  $h_{ingot} = \varepsilon_1 \sigma (T_1^2 + T_2^2)(T_1 + T_2).$

Finally, concerning the crucible, exterior boundaries will be cooled by different mean. Heat transfer coefficient is obtained from the "Heat Transfer module" of COMSOL Multiphysics® for natural convection with air. If forced convection (water cooling) is modeled, heat transfer coefficient is obtained from the literature for lateral and bottom surfaces [3].

The latent heat of solidification is added through the "Phase Change Material" Interface for Fluid Domain in the "Heat Transfer" node. Although radiation between the ingot upper surface and ambient could be an important effect, it is not considered in this simplified model. It has been implemented in a more complete model, not presented here.

Metallurgy

As explained previously, the metallurgical phase composition of the metal ingot is directly influenced by its thermal history over time and the properties of each potential phase change. The example of low-alloy steel is detailed in this part. A continuous cooling transformation diagram (CCT), illustrated in Figure 2, can be used to describe the evolution of the different metallurgical phases. Initially the metallurgical state is assumed to be only composed of austenite phase.
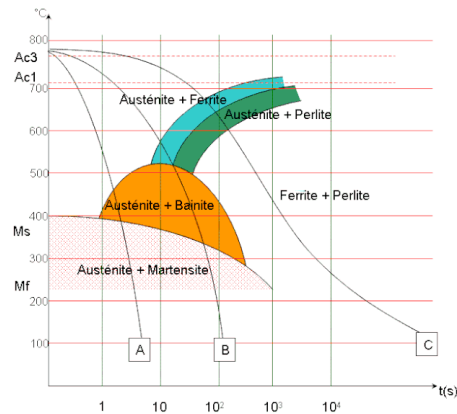

Figure 2. CCT diagram from [4]

Two types of evolution are classically distinguished in metallurgy and modeled in this work.

First of all, transformation from austenite to ferrite and/or pearlite is unified into a singular phase transition. Given its diffusive behavior, this transformation is represented using the Leblond-Devaux phase transformation model [3]. The temperature-dependent functions ($K_i(T)$ and $L_i(T)$) that describe this phase transformation are obtained from [4]. The rate at which the fraction of the ferrite and pearlite phases (formed at the expense of the austenite phase) changes over time, is then given by:

$$\dot{z}_i = K_i(T)z_{austenite} - L_i(T)z_i \qquad \text{Eq. 4}$$

with z_i the fraction of phase i (ferrite and pearlite) and $z_{austenite}$ the austenite fraction.

For the bainite formation, the same diffusion mechanism process is modeled, but including a dependency on the temperature rate [3]. By using the

same functions presented in [4], the following equation is added:

$$\dot{z}_{bainite} = F(T)H(\dot{T})z_{austenite} - G(T)H(\dot{T})z_{bainite} \qquad Eq.\ 5$$

with $z_{bainite}$ the bainite phase fraction.

Second of all, in contrast to the diffusive phase transformations discussed earlier, the martensitic phase transformation is characterized by a displacive mechanism [5]. The amount of martensite formed is directly linked to the degree of undercooling below the martensite start temperature (M_s). This transformation is well approximated using the Koistinen-Marburger model, as referenced in [5]. The rate at which the transformation progresses, leading to the formation of the martensite, can be expressed as follows if $\dot{T} < 0$ and $T < M_s$:

$$\dot{z}_{martensite} = -z_{austenite}\beta\dot{T} \qquad Eq.\ 6$$

with $z_{martensite}$ the martensite phase fraction and β a growth factor obtained from [4].

Solid and thermal material properties could vary with the proportion of each metallurgical phase, but it is not considered in this work.

Solid Mechanics
At high temperatures, the behavior of materials is highly non-linear and viscoplastic effects have to be taken into account to estimate stress and strain states. Firstly, the strain tensor ($\underline{\underline{\varepsilon}}$) is classically shared in two parts: the elastic strain tensor ($\underline{\underline{\varepsilon}}^e$) and the plastic tensor ($\underline{\underline{\varepsilon}}^p$):

$$\underline{\underline{\varepsilon}} = \underline{\underline{\varepsilon}}^e + \underline{\underline{\varepsilon}}^p \qquad Eq.\ 7$$

Secondly, constitutive relation between the stress tensor ($\underline{\underline{\sigma}}$) and the strain tensors, is expressed as follows, taking into account the thermal expansion:

$$\underline{\underline{\sigma}} = \mathbb{E}(T):\left(\underline{\underline{\varepsilon}} - \underline{\underline{\varepsilon}}^p - \alpha(T,z_i)\cdot(T-T_0)\underline{\underline{I}}\right) \qquad Eq.\ 8$$

with $\mathbb{E}(T)$, the 4th-order elasticity tensor function of $E(T)$, the Young modulus and $\nu(T)$ the Poisson coefficient; $\alpha(T,z_i)$, the coefficient of thermal expansion and T_0 a reference temperature.

The "Lemaitre and Chaboche" model [1] is used here to describe viscoplastic flow and non-linear hardening. In this work, only the kinematic hardening is considered. A "back stress" tensor, $\underline{\underline{X}}$, is defined, linked to the plastic strain rate tensor $\underline{\underline{\dot{\varepsilon}^p}}$ and the effective strain rate $\dot{p}$. The complete system of equations which describes this viscoplastic flow with non-linear kinematic hardening is expressed by:

$$\underline{\underline{\dot{\varepsilon}^p}} = \dot{p}\frac{3}{2}\frac{\underline{\underline{\sigma}}' - \underline{\underline{X}}'}{J_2\left(\underline{\underline{\sigma}}' - \underline{\underline{X}}'\right)} \qquad Eq.\ 9$$

$$\underline{\underline{\dot{X}}} = \frac{2}{3}C(T)\underline{\underline{\dot{\varepsilon}^p}} - \gamma\underline{\underline{X}}\dot{p} \qquad Eq.\ 10$$

$$\dot{p} = \left(\frac{\left\langle J_2\left(\underline{\underline{\sigma}} - \underline{\underline{X}}\right) - \sigma_y(T)\right\rangle}{K(T)}\right)^{n(T)} \qquad Eq.\ 11$$

with $\sigma_y(T)$, the yield stress, $C(T)$ and γ, two kinematic hardening coefficients and $K(T,z_i)$ and $n(T,z_i)$, two coefficients of viscoplasticity.

The notation $\underline{\underline{A}}'$ represents the deviatoric part of a tensor $\underline{\underline{A}}$. The bracket notation $\langle A \rangle$ is the positive part of A and the J_2 notation is the second deviator invariant of the considered tensor.

At last, the quasi-static equation of motion is solved for by using the "Solid Mechanics" physics:

$$\nabla\cdot\underline{\underline{\sigma}} = 0 \qquad Eq.\ 12$$

Deformed Geometry
In order to model the ingot growth, a deformed geometry is used. The velocity is analytically known in this approach and the resulting variation of height can be directly computed with the following relation:

$$\Delta Z = \frac{\left(v_{ingot}\cdot t\cdot f(t) + h_{ingot}(1-f(t))\right)\cdot Z}{h_{ingot}} \qquad Eq.\ 13$$

with v_{lingot} is the known velocity of the ingot surface (resulting of the casting velocity or the melting velocity of an electrode for example), $f(t)$ is a step function equals to 1 during the casting and 0 after and h_{ingot} the initial height of the ingot.

Model Validation / Numerical Aspects

All the previous equations are solved together, with a segregated approach. Indeed, the couplings between all these phenomena are mostly in one direction and no specific convergence issues have been encountered. Concerning the spatial discretization, a mapped mesh is used, and 2nd order of Lagrange polynomials are used for the discretization of each variable. The maximum time step is controlled and limited in the BDF solver.

In order to study the precision of our approach, mass and energy balances are good indicators to validate numerical parameters. As the geometry is analytically controlled, the mass balance is trivial. An energy balance is also performed and shown in Figure 3. It represents the evolution of both cooling powers (lateral in blue and bottom in green) and the

resulting enthalpy variation (in red). With cyan markers the opposite of the sum of these cooling powers is plotted, showing a very good correlation with enthalpy variation and highlighting the complete energy balance validity.
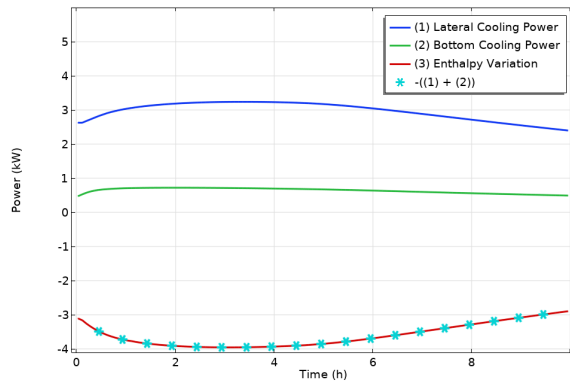

Figure 3. Energy Balance

This result numerically validates the model. It will now be used in different operating conditions to study the influence of cooling conditions and the importance of contact boundary conditions.

Results

Thermo-mechanical Results

As discussed previously, a major advantage of this thermo-mechanical model is that it enables us to study the contact between the ingot and the crucible in greater detail. A study case is performed with a natural convection cooling and with an ingot growth time of half an hour. The resulting shape of the ingot is shown (with a deformation factor of 10 for thermal dilatations) at different instants in Figure 4. During the growth phase ($t \leq 1800s$), the melting zone is delimited by the isotherm $T = T_{melting}$, plotted in magenta contour. The heat shrinkage zone can be observed from the start of the ingot growth and increases with time (see Figure 4). When the growth is stopped ($t = 1800s$), the ingot cools down and the resulting shape of the ingot is obtained, depending directly on the dilatation coefficient.
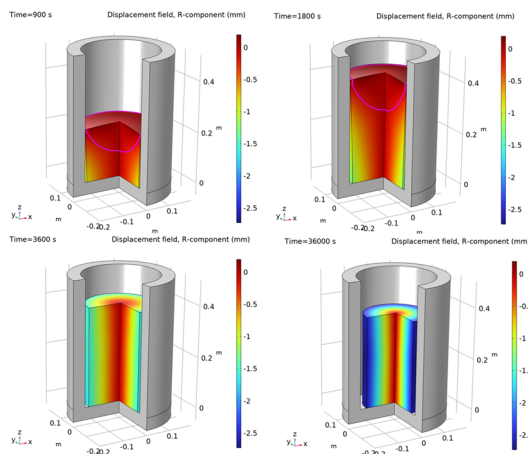

Figure 4. Radial displacement due to thermal dilatation at different instants (deformed view by a factor10)

Residual stresses can also be estimated with this approach. A representation is given in Figure 5 during the growth phase ($t = 900s$) and at the end of the cooling ($t = 36000s$). Depending on the cooling kinetics, high values can be observed given valuable information for the life of the ingot.
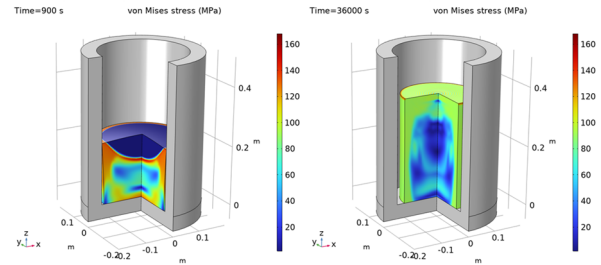

Figure 5. Von Mises stresses at different instants (deformed view by a factor10)

Thermal Exchanges

As explained previously, the value of the conductance at the ingot/crucible interface, h_{ingot} is not well known. It depends mainly on the local properties of the surfaces, the contact pressure, and the mechanical properties of the ingot boundary. This approach gives a first approach of the contact size by considering the mechanical behavior of the ingot during the growth. Three values are studied to quantify the influence of this parameter by plotting the temperature at the top boundary and at the center of the ingot (Figure 6). The higher the conductance, the greater the exchange with the crucible and the faster the cooling. Contact resistances relations, given by COMSOL Multiphysics® using Mikic's assumptions [8] and functions of the local contact pressure, will be studied in a future work to provide a more predictive model.
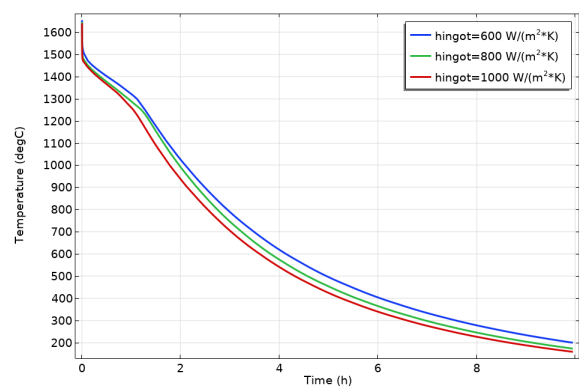

Figure 6. Temperature evolution at the top boundary and at $r = 0$ in the ingot for three values of h_{ingot}

Another very important mechanism is obviously the mode of cooling of the crucible. Indeed, depending on the type of casting, the crucible can be designed as a good heat conductor to benefit from forced convection cooling, or as a thermal insulator to control the cooling with natural convection only. Two types of convection at the periphery of the crucible are studied here by plotting the temperature

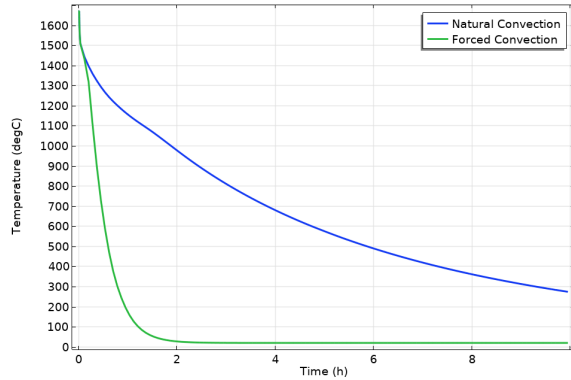evolution at the top boundary and at the center of the ingot (Figure 7).

Figure 7. Temperature evolution at the top boundary and at $r = 0$ in the ingot for two types of cooling

As expected, with forced convection by water flow, cooling kinetics are higher. This parametric study emphasizes the importance of a precise modeling of this effect. Thanks to temperature evolution prediction, the resulting metallurgy of the ingot can now be studied into more details.

Metallurgical Results

As explained previously the metallurgical state highly depends on the temperature and the cooling rate. An illustration of the ability of the model to predict the formation of each metallic phase is shown by plotting the four phases generated from austenite initial phase, at $(t = 4h)$ in Figure 8, and after cooling $(t = 10h)$ in Figure 9. At $t = 4h$, formation of pearlite and ferrite begins from the top of the ingot and follows temperature gradients. At the end of the cooling, each phase is mostly spatially constant (adapted scales have been used to illustrate local variations in Figure 9).
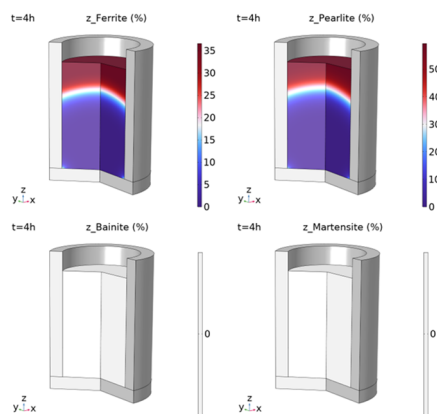

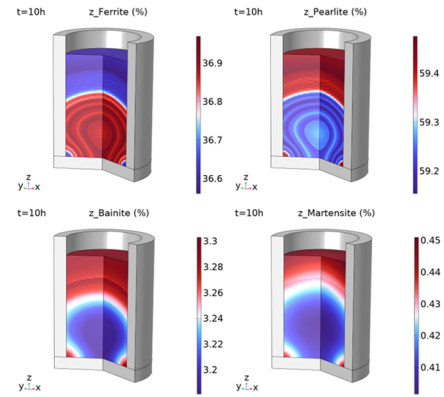*Figure 8. Metallurgic phases after 4 hours under slow cooling conditions*

Figure 9. Metallurgic phases at the end of the cooling phase under slow cooling conditions

Both same previous cooling conditions are simulated (natural and forced convection mode), and metallurgical results are shown in terms of phase fraction at the top boundary and at the center of the ingot. As expected, for slow cooling Figure 10, the predominant phase to form after cooling is pearlite. Slow cooling allows the atoms in the steel to diffuse slowly and form lamellar structures of ferrite and cementite, which together make up pearlite. On the other hand, for a faster cooling (see results in Figure 11) bainite forms as well as a small fraction of martensite. Because it is a phase transformation without diffusion, martensite forms at higher cooling kinetics and a higher fraction could be achieved by increasing kinetics. In this case, the high concentration of bainite (Figure 11) indicates that the cooling is an intermediate cooling rate.
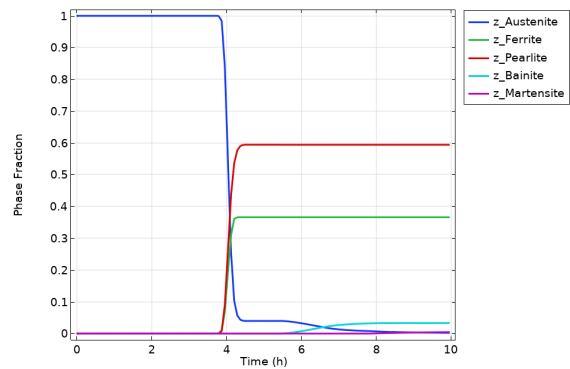

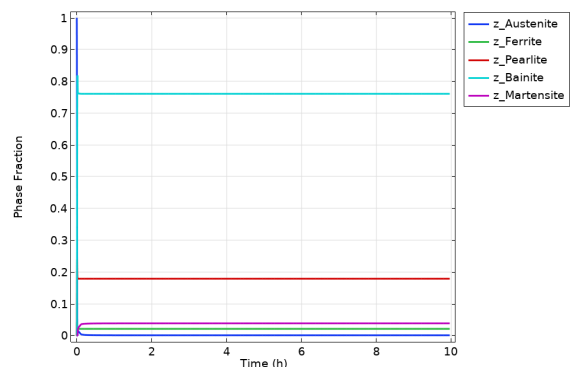*Figure 10. Metallurgic phases evolution for low cooling velocity*

Figure 11. Metallurgic phases evolution for high cooling velocity

Conclusions

A thermo-metallo-mechanical model has been developed in this paper to study the influence of ingot cooling under different operating conditions. After a concise description of the main assumptions, the model has been detailed and then validated with an energy balance.

Thermal, mechanical, and metallurgical results have been discussed to highlight the interest of such model and the importance of the control of cooling conditions. This first approach is very promising because it provides new information for predicting the contact zone dimensions. A first step towards the prediction of the conductance between the ingot and the crucible has been taken and the study will continue in a future work. This major aspect will be added to other numerical approaches adapted to specific foundry processes and experimental measurements would be developed to validate these results.

References

[1] J. Lemaitre et J.-L. Chaboche, Mécanique des matériaux solides, Dunod, 2001.

[2] T. Quatravaux, Évolution de la modélisation du procédé VAR : contribution à la description de la dispersion inclusionnaire dans le puits liquide et à la prévention de défauts de solidification, Nancy, 2004.

[3] W. H. McAdams, "Review and summary of developments in heat transfer by conduction and convection.," *Transactions of the AIChE,* vol. 36, pp. 1-20, 1940.

[4] "www.wikipedia.fr," [Online].

[5] J. Leblond and J. Devaux, "A new kinetic model for anisothermal metallurgical transformations in steels including effect of austenite grain size," *Acta Metall.,* vol. 32, no. 1, p. 137–146, 1984.

[6] Comsol Multiphysics, Phase Transformations in a Round Bar.

[7] D. Koistinen and R. Marburger, "A general equation prescribing the extent of the austenite-martensite transformation in pure iron-carbon alloys and plain carbon steels," *Acta Metall.,* vol. 7, p. 59–60, 1959.

[8] B. Mikic, "Thermal contact resistance; Theoretical considerations," *Int J. Heat Mass Transfer,* vol. 17, pp. 205-214, 1974.